MECHANISM OF EARTH PRESSURE ACING ON SEMI-UNDERGROUND STRUCTURE DURING AND AFTER EARTHQUAKE

T.Igarashi[(1)], S.Sawada[(2)], H.Goto[(3)]

[(1)] *Director, Corporate Reforms Department, NEWJEC. Inc., igarashitr@newjec.co.jp*
[(2)] *Professor, Disaster Prevention Research Institute, Kyoto University, sawada@catfish.dpri.kyoto-u.ac.jp*
[(3)] *Associate professor, Disaster Prevention Research Institute, Kyoto University, goto@catfish.dpri.kyoto-u.ac.jp*

Abstract

Water supply facilities are one of the extremely important utilities that are indispensable for daily life and continuation of advanced socio-economic activities. These facilities are required to maintain their function even in the event of a large-scale earthquake. Seismic resistance evaluation and reinforcement work have been promoted for many water supply facilities. A major structural type of water storage units is semi-underground structures. Most part of their bodies is embedded in the underground, and the roofs are covered with thin or no soil layers. These structures are lighter and stiffer than the surrounding soil. The current earthquake design standard for semi-underground structures mainly considers the earth pressure which is proportional to ground acceleration and displacement. However, detailed mechanisms of active and passive earth pressures are not considered in the current design method.

The dynamic interaction mechanism between ground and side wall of semi-underground structures during earthquakes is studied using FEM analysis. Non-linear soil-structure interaction is examined, focusing on the stress state of the surrounding soil and the earth pressure acting against the side wall, during and after earthquakes. Parameter study has been performed considering the surface layer thickness, structural depth, and predominant period and amplitude of input motion. It is observed that the depth-wise distribution of the horizontal stress is not affected by the surface soil thickness. Also, the amplitude of input motion determines the area in which the passive earth pressure acts, whereas its period has little effect on the distribution. The results show that passive earth pressure acts on the shallow part of the wall whereas active earth pressure acts on the deeper part, during earthquake. The residual earth pressure, which is approximately the median value of active and passive earth pressure, acts after earthquake.

It is found that the conventional design methods could not represent the complex distribution of earth pressure acting on the semi-underground structure. The conclusion is examined using the practical conditions of soils and structures against the ground motion records during the 1995 Kobe earthquake.

Keywords: Semi-underground structure; Soil-Structure Interaction; Earth pressure; Shear-failures; FEM analysis

1. Introduction

Water supply facilities are one of the lifelines indispensable for daily life and socio-economic activities. Seismic design of these structures is very important to maintain serviceability during and after large earthquakes. There are different structural types in water supply facilities, namely above-ground, underground and semi-underground structures, as illustrated in Fig.1(a), (b) and (c). Water reservoir tanks installed on hills are representative examples of above-ground structures (Fig.1(a)). Note that in this paper the standard retaining walls are categorized as above-ground structures. Buried pipe-lines, vertical shafts and utility corridors are distinguished as underground structures (Fig.1(b)). Semi-underground structures, for example water reservoirs, are often constructed having most part of the structure placed underground and the roofs are covered with thin or no soil layers (Fig.1(c)). Difference between the semi-underground structures and the standard retaining wall is in the rigidity of the walls against surrounding grounds.

During earthquakes, the above-ground structures are mainly affected by their inertia forces; this is known as "inertia interaction". The seismic force is generally given by the product of mass and total of ground and structural response acceleration. In static design procedure, such as the "seismic coefficient method" proposed by Sano [1], the seismic force is assumed as the product of the weight and seismic coefficient. For the design of ground slope and/or retaining wall, the active soil block is assumed accoding to the slip failure plane at limit equilibrium; this is called the "Mononobe - Okabe method" proposed by Okabe, Mononobe and Matsuo [2] [3]. The reaction force acting on the retaining wall is restricted to the active earth pressure because the wall is easily deformed by the movement of soil block. Note that the reaction force gets larger as the overburden soil thickness increases [4], because the active pressure is proportional to the overburden pressure (Fig.2(a)). Koseki et al. [5] proposed "Modified Mononobe – Okabe method" in which the failure plane is determined at the instant when the failure first occurs, based on the stability analyses of damaged retaining walls during the 1995 Kobe earthquake. This method is widely used for the static design of retaining walls [6] [7].

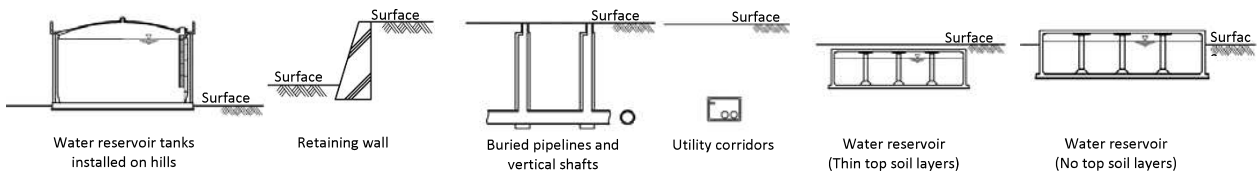

(a) Above-ground structures (b) Underground structures (c) Semi-underground

Fig. 1– Structural types

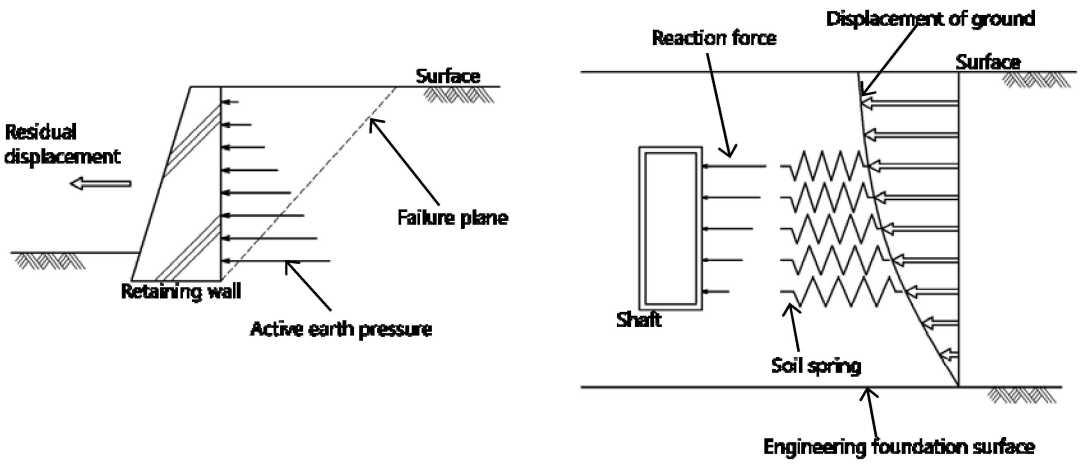

(a) Seismic coefficient method for retaining wall (b) Seismic deformation method for shaft

Fig. 2– The reaction force assumed in static design methods

The underground structures are predominantly influenced by the surrounding soil due to "kinematic interaction". Previous studies show that the structural deformation depends on the difference of rigidity and weight between the ground and the structure [8]. Static and dynamic earth pressures acting on the underground structure are the main external forces for structural design. Static analyses are often used to evaluate the earth pressure during earthquake. One of these methods is "ground response acceleration method", which models the soil-structure interaction (SSI) using static FEM, where the inertia force is given by the individual dynamic ground response analyses [9]. Another method is the "seismic deformation method" in which structural beam and soil spring are often used for modeling, and the maximum displacements of free-field ground are inputted statically to the soil spring [10]. In this method, the resulting reaction force against the structure decreases as the overburden soil thickness increases (Fig.2(b)). Note that the failure plane in the ground is not assumed, whereas the stiffness of soil spring is reduced in accordance with its plasticity [11]. Inertia force, which is calculated based on the difference between structure and soil weights, is also considered.

A few studies [12, 13, 14, 15, 16] have been performed for semi-underground structures which are stiffer than the surrounding soil. However, standard design method for semi-ground structures have not been developed yet [17]. Igarashi et al. [18] studied the mechanism of dynamic interaction between ground and side wall of semi-underground structures based on a two-dimensional FEM analysis. Igarashi et al. examine non-linear SSI, focusing on the stress state of the surrounding soil and the earth pressure acting against the side wall, during and after earthquake. The following effects are investigated; soil failure, thickness of surface layer, depth of structure and period and amplitude of the input motion.

In this study, the results of conventional design method are compared with the earth pressure obtained by non-linear FEM in order to study whether the conventional design methods can represent the complex distribution of earth pressure acting on the semi-underground structure. The maximum and residual distributions of earth pressure during earthquakes are also examined using the practical conditions.

2. Model Analyzed [18]

Igarashi et al. examined non-linear SSI, focusing on the stress state of the surrounding soil and the earth pressure acting against the side wall. The semi-underground structure and surrounding ground are analyzed using the computer program TDAP III (ARK Information Systems, Inc.) which is based on a two-dimensional plane-strain dynamic FEM. Fig.3 shows the model analyzed. The top of the model is a free surface whereas the sides and the bottom are viscous boundaries. The width of the main area under analysis is 30m. It includes a 10m wide structure, accompanied by 40m wide side areas to eliminate the boundary effects. The side walls and bottom slab of the structure consist of rigid beams which are connected to the soil elements using the normal and shear springs The rigidity of the shear springs on the walls are set to small values (~ 10^{-8}) to simulate slippage between the walls and soil, whereas the rigidity of other shear and normal springs are set to large values (~ 10^{12}) to prevent slippage, separation and invasion.

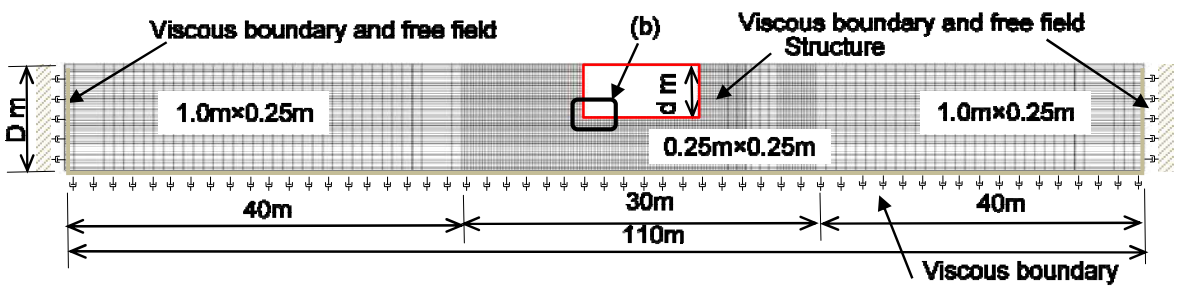

Fig. 3– Analysis model [18]

Analysis is performed on 11 cases as listed in Table 1. The surface layer thickness, D, is set between 7.5 and 20 m. The shear-wave velocity of surrounding soil, Vs, is 151.5 m/s. The natural period of the ground is 0.264 s which is calculated by the quarter-wavelength law for the cases of D=10 m. To keep the calculation stable, cohesion, C, of 3 kPa in the failure criteria and 3% of damping factor [19] set at 1 and 10 Hz based on Rayleigh damping, are introduced. Note that large damping ratio may give inadequate solutions during convergence calculation for nonlinear constitutive model. The damping values used has been properly confirmed.

Linear soil cases are also calculated to examine the effect of structure mass and to compare the soil failure cases, in which a non-mass case "Li-D10-d05-T1.0-0.3g" and a half-mass case "Li-D10-d05-T1.0-0.3g-M50%" whose structural densities are respectively 0% and 50% of the soil density are adopted. Two semi-underground structures with depths, d, of 5 and 10 m, are simulated. Horizontal motion is applied through the bottom viscous boundary and its amplitude is adjusted to make the surface ground response acceleration attain the following values: 0.1 g for the case "MC-D10-d05-T1.0-0.1g", 0.5 g for the case "MC-D10-d05-T1.0-0.5g", and 0.3 g for all the other cases. Note that the damping factor has little effect on the results because the amplitude of input motion is adjusted by the surface ground response.

The input waveform consists of 8-cycles of sine wave accompanied with 3-cycles of increasing and decreasing sections, as shown in Fig.4(a). In this study, we define four important instants as follows: T_{ini} representing the state before shaking, T_{pas} for passive state on right area of surrounding soil, T_{act} for active state on the right area of surrounding soil, and T_{aft} for the state after shaking. Fig.4(b) shows the image of deformation at T_{pas}. At T_{pas}, the right area of surrounding soil (except the deep part) attached to the right wall of the semi-underground structure, is compressed laterally, where σ_x increases and passive earth pressure acts against the right wall. In contrast, the left area is simultaneously tensioned laterally where σ_x decreases and active earth pressure acts against the left wall. At T_{act}, reversal of the tensile and compression areas take place.

Table 1 – Specifications Applied to the Analysis [18]

Case	Soil material					Structure		Ground		Imput motion	
	Common parameters		non-linear model	Cohesion C (kPa)	Friction angle ϕ (degree)	Unit volume weight (tf/m^3)	Structure depth d (m)	Surface layer thickness D (m)	Natural period of ground (s)	Period of motion T (s)	Peak ground acceleration (g)
Li-D10-d05-T1.0-0.3g-M50% (Half mass case)	Unit volume weight	1.7 (tf/m^3)	Linear	–	–	0.85	5	10.0	0.264	0.264	0.3
Li-D10-d05-T1.0-0.3g						0.0					
MC-D7.5-d05-T1.0-0.3g	Shear modulus G	3.903×10^4 (kN/m^2)	Perfect elasto-plasticity	3	30		5	7.5	0.198	0.198	
MC-D10-d05-T0.5-0.3g (Half period case)								10.0	0.264	0.132	
MC-D10-d05-T0.5-0.3g (Basic case)	Poisson's ratio ν	0.33								0.264	
MC-D10-d05-T1.0-0.1g											0.1
MC-D10-d05-T1.0-0.5g	Damping ratio	3 (%)									0.5
MC-D15-d05-T1.0-0.3g								15.0	0.396	0.396	0.3
MC-D20-d05-T1.0-0.3g	Shear wave velocity Vs	151.5 (m/s)						20.0	0.528	0.528	
MC-D15-d10-T1.0-0.3g							10	15.0	0.396	0.396	
MC-D20-d10-T1.0-0.3g								20.0	0.528	0.528	

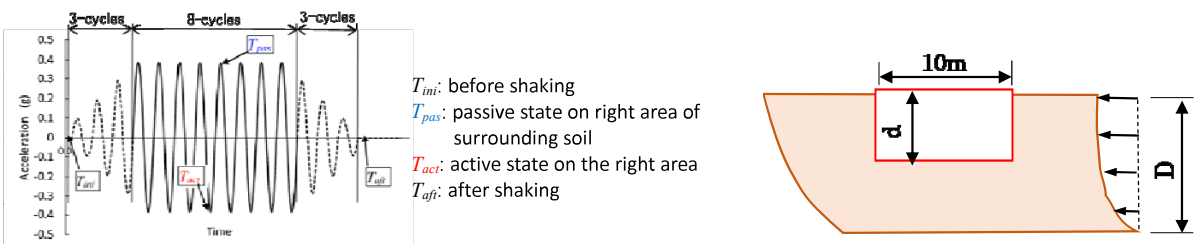

(a) Input waveform and four important instances[18]

(b) The image of deformationation at T_{pas}.

Fig. 4– Simulation model and Input waveform.

3. Stress Distribution During and After Shaking [18]

Linear soil cases are investigated to examine the effect of structural mass and to compare with the soil failure cases. Fig.5(a) shows spatial distributions of horizontal stress (σ_x), normalized by the initial values (σ_{x0}), at the four important instances instants for the non-mass case "Li-D10-d05-T1.0-0.3g". The red and blue colors represent the active ($\sigma_x < \sigma_{x0}$) and passive ($\sigma_x > \sigma_{x0}$) areas, respectively. The distribution pattern at T_{act} is symmetrical to that at T_{pas}. The stress value after shaking is restored to the initial value because it is a linear case. Fig.5(b) shows the distributions of σ_x with depth at the four instances, where σ_x is earth pressure acting on the right wall of the structure and its extended deeper plane. The black solid line represents the stress distribution of σ_x at T_{ini}, which marks the boundary between the passive state on the right and active state on the left. The gray dashed lines, representing the theoretical active and passive earth pressure, are shown as auxiliaries to compare σ_x with the non-linear cases. The blue solid and dashed lines are the stress distributions at T_{pas} for the non-mass case "Li-D10-d05-T1.0-0.3g"and half-mass case "Li-D10-d05-T1.0-0.3g-M50%", respectively. The red solid and dashed lines are the stress distributions at T_{act} for these cases. It is shown that the effects of dynamic SSI are larger in the non-mass case than in the half-mass case. As we focus on the mechanism of earth pressure during earthquake in this paper, only non-mass condition, giving largest effects of dynamic SSI, is adopted for the non-linear cases.

Fig.6(a) shows the spatial distribution of normalized horizontal stress for a non-linear soil case "MC-D10-d05-T1.0-0.3g", which is the basic case for the following comparison. The area in active state (shown in red) at T_{act} is smaller than that of the linear case shown in Fig.5(a). The distribution at T_{pas} is symmetrical to that at T_{act}. The stress values at T_{aft} do not return to the initial values and have residual stresses which are passive in the shallow area and active in the deep area. Fig.6(b) plots the distributions of σ_x with depth. It is shown that the horizontal stress is restricted along the theoretical lines of passive and active earth pressure, especially at shallow and deep locations, respectively. The horizontal stress at T_{aft} stays passive in the shallow area where the depth is less than about 3 m, whereas in the deeper part the stress is in active state during and after shaking except just near the structural bottom.

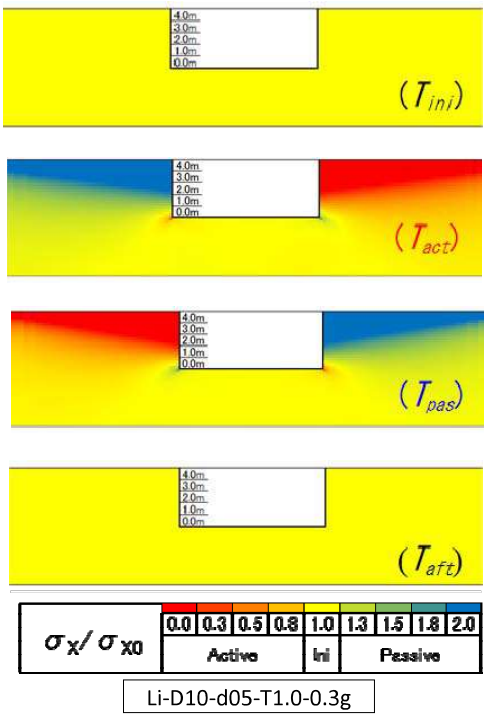

(a) Spatial distributions of σ_x/σ_{x0} at the four instances for linear non-mass case

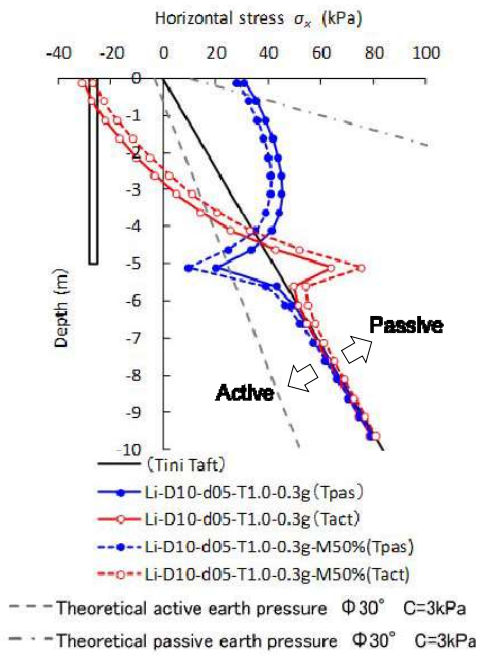

(b) Depth-wise distributions of σ_x at the four instances for linear non-mass case and half-mass case acting on the right wall and its extended deeper plane

Fig. 5– Distribution of horizontal stress (σ_x) for linear cases [18].

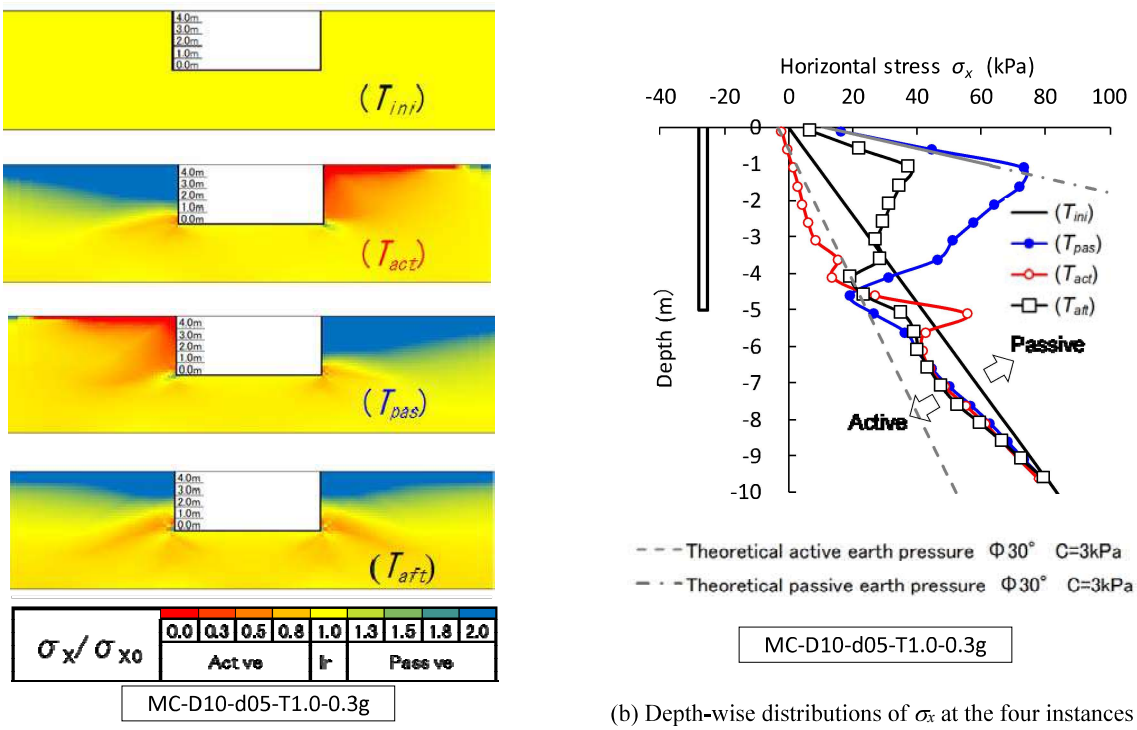

(a) Spatial distributions of σ_x/σ_{x0} at the four instances for basic case

(b) Depth-wise distributions of σ_x at the four instances for acting on the right wall and its extended deeper plane

Fig. 6– Distribution of horizontal stress (σ_x) for basic cases [18].

3. Effects of Soil and Structure Conditions [18]

Four cases with varying surface layer thickness of D=7.5, 10, 15 and 20 m are examined keeping the depth of structure (d) fixed at 5 m. Fig.8(a) and (b) shows the depth distribution of horizontal stress for the cases of D=7.5 m "MC-D7.5-d05-T1.0-0.3g" and D=20 m "MC-D20-d05-T1.0-0.3g", respectively. Five more cases are additionally generated by combining structural depth d=5 and 10 m, with surface layer thickness D=10, 15 and 20 m, except the case of d=10 m and D=10 m.

Fig.8(a) compares depth-wise distribution of σ_x at T_{pas}, where the solid lines and dashed lines represent the results with structural depth d=5 m and d=10 m, respectively. It is observed that the distribution of horizontal stresses at T_{pas} have no significant difference between all the cases with the same structural depth.

Fig.8(b) is converted from Fig.8(a) to emphasize the effects of structural and soil depth. The vertical axis is normalized by structural depth. The horizontal axis is also converted to Rankine's coefficient of earth pressure, using the ratio of $\sigma_x+C\cot\phi$ and $\sigma_{y0}+C\cot\phi$, where $C\cot\phi$ is added to consider the cohesion. Note that the Rankine's coefficient of passive and active earth pressure, K_p (= $(1+\sin\phi)/(1-\sin\phi)$) and K_a (= $(1-\sin\phi)/(1+\sin\phi)$), are 3.0 and 0.33, respectively, when the friction angle ϕ is 30 degrees without cohesion. Normalization in structural depth results in the single distribution for all cases. The peak value of earth pressure agrees well with K_p indicated by the blue chain line, at an area shallower than 20% of structural depth. Smallest value of earth pressure is regulated with K_a shown by the red dashed line, which appears at around the structural bottom. No significant effect of surface layer thickness is observed.

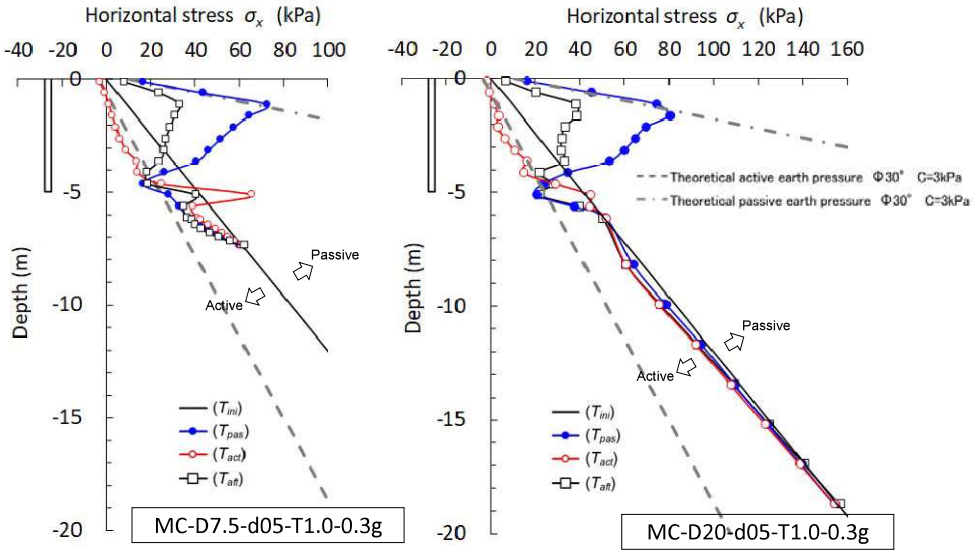

(a) Thin surface layer (D= 7.5 m) (b) Thick surface layer (D= 20 m)

Fig. 7– Depth-wise distributions of σ_x at the four instances for the different surface layer cases [18].

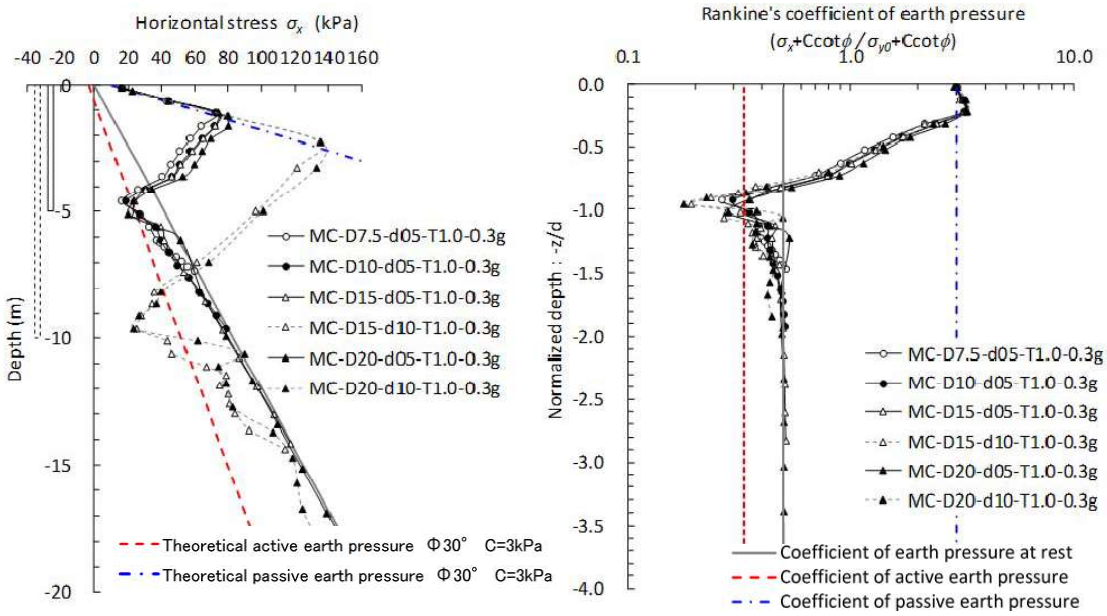

(a) Horizontal stress σ_x at T_{pas} (b) Rankine's coefficient of residual earth pressure (σ_x +Ccotϕ / σ_{xy0}+Ccotϕ)

Fig. 8– Depth-wise distributions of earth pressure at the T_{pas} for different surface layers and structural depths [18].

5. Effects of Input Motion [18]

To examine the effect of resonance in surface layer, case "MC-D10-d05-T0.5-0.3g" is designed. In this case, a short-period motion (t=0.132 s) is inputted to compare with the basic case "MC-D10-d05-T1.0-0.3g". Fig.9(a) shows the distribution of horizontal stress σ_x with depth for comparing with Fig.6(b). Fig.9(b)

shows the normalized comparison at T_{pas} as defined in the previous section. The open circles and the filled circles represent the results of short-period case and the basic case, respectively. No significant difference is seen in the figure, because the amplitude of the motion is regulated by the same acceleration value on ground surface.

Additional two cases with different amplitudes of input motion, the case "MC-D10-d05-T1.0-0.1g" with 0.1 g and the case "MC-D10-d05-T1.0-0.5g" with 0.5 g, are analyzed and compared with the basic case "MC-D10-d05-T1.0-0.3g" with 0.3 g. Fig.10(a), (b) shows the depth-wise distribution of σ_x for the cases of 0.1 g and 0.5 g, respectively, to compare with Fig.6(b). For the 0.1 g case, only active failure occurs. Fig.10(c) shows the normalized comparison at T_{pas} using Rankine's coefficient and structural depth. The open triangles, open circles and cross marks represent the result of 0.1 g, 0.3 g and 0.5 g, respectively. The thicknesses giving the passive earth pressure is controlled by the amplitude of input motion, whereas the coefficient near the structural bottom varies in active state.

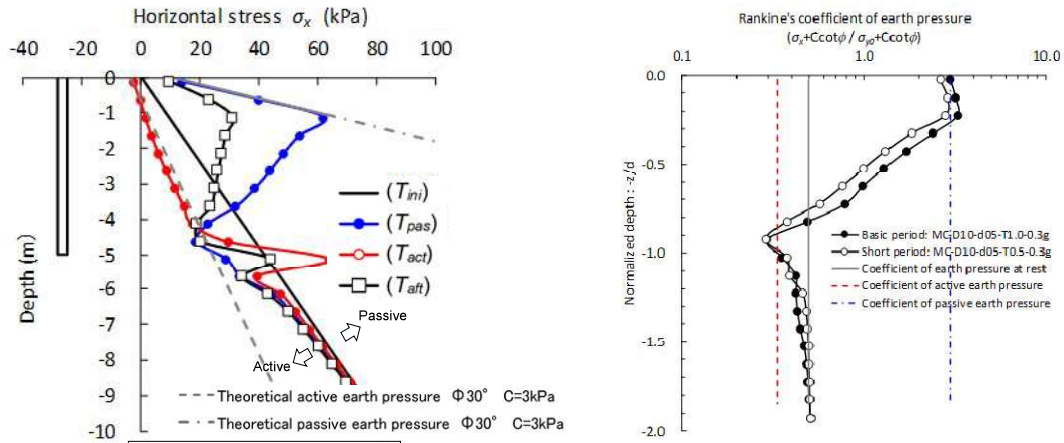

(a) Horizontal stress σ_x

(b) Rankine's coefficient of earth pressure at the T_{pas} for different period of input motion.

Fig. 9– Depth-wise distributions of σ_x at the four instances for the case of short-period input motion and Rankine's coefficient of earth pressure at the T_{pas} for different period of input motion [18].

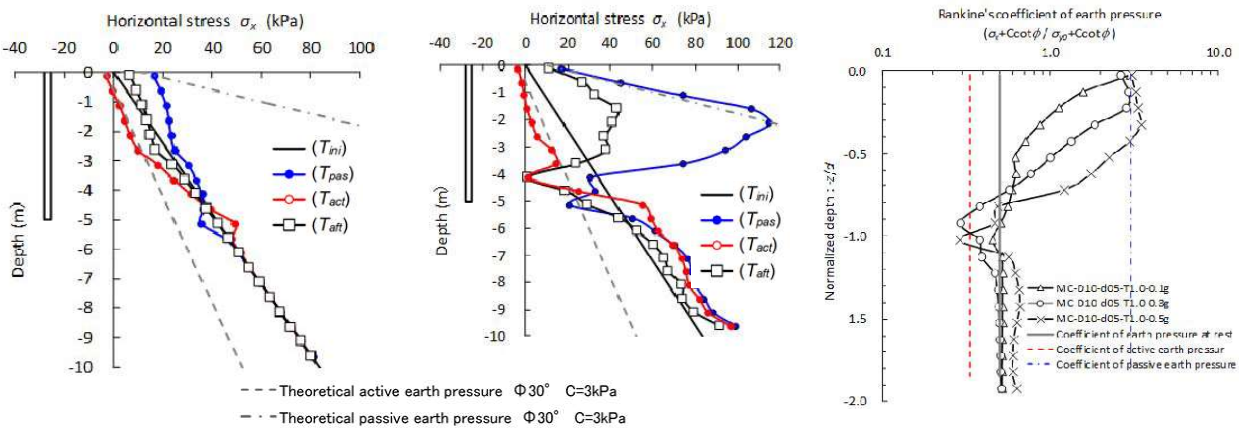

(a) Case of 0.1g

(b) Case of 0.5g

(c) Rankine's coefficient of earth pressure at the T_{pas} for different amplitudes.

Fig. 10– Depth-wise distributions of σ_x at the four instances and Rankine's coefficient of earth pressure at the T_{pas} for different amplitudes [18].

6. Comparison with Conventional Design Methods

Fig.11 shows the comparison between the distributions of horizontal stress σ_x resulted by FEM and conventional desgin methods, those are "Modified Mononobe – Okabe method" and "seismic deformation method" represented by red and purple lines, respectively. The blue dashed and solid lines are the stress distributions at T_{pas} for the linear case "MC-D10-d05-T1.0-0.3g"and non-linear case "Li-D10-d05-T1.0-0.3g", respectively. The black solid line represents the initial stress distribution of σ_x. The gray dashed lines represent the theoretical active and passive earth pressure, respectively. It is shown that the conventional design methods could not represent the complex distribution of earth pressure acting on the semi-underground structure obtained by non-linear FEM.

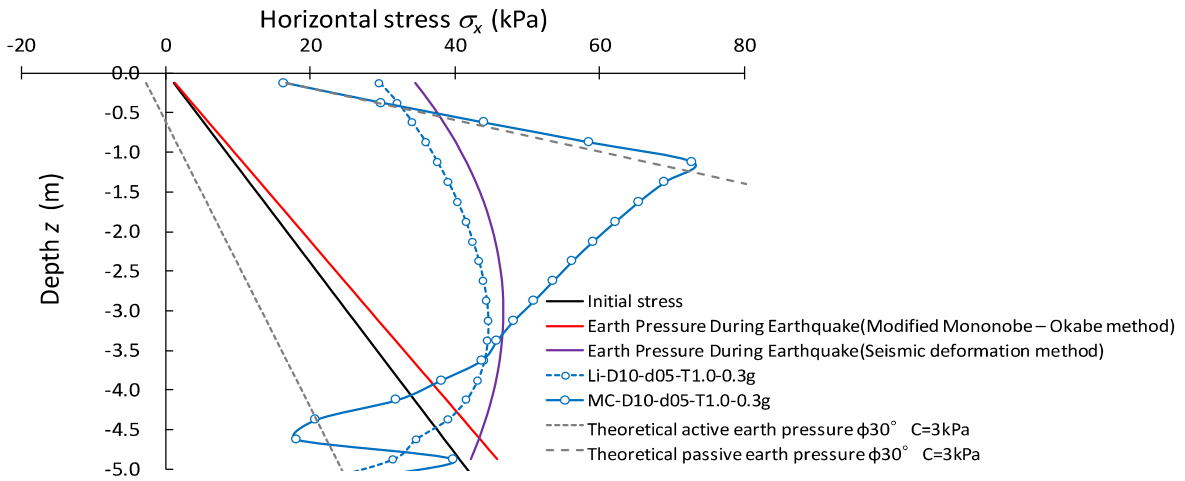

Fig. 11– Depth-wise distributions of σ_x for for comparing with conventional desgin methods

7. Examination under practical conditions

The distributions of horizontal stress σ_x with depth is examined using the practical conditions. Specifications used are listed in Table 2. The soil layers are modeled with reference to the soil profile at Daikai station [20], which was damaged due to the 1995 Kobe earthquake. Horizontal motion applied is the record at Takatori station during the earthquake [21], where is categorized into the same ground group with Daikai station. Note that its amplitude is scaled to make the surface ground acceleration 0.3 g.

Fig.12 shows the depth distribution of horizontal stress for the practical conditions. The blue line with open circles represents the stress distribution at the instant when the maximum earth pressure occurs. The black line with open rectangles is the distribution after earthquake. It is shown that the horizontal stress is restricted by the theoretical lines of passive pressure, especially at shallow area. The horizontal stress after earthquake stays passive in the shallow area where the depth is less than about 2.5 m, whereas in the deeper part the stress is in active state after earthquake except just near the structural bottom. These tendencies are the same with the results of simple conditions mentioned before.

Table 2 – Specifications used for the examination

Level	Layers thickness	Soil material			Structure			Peak ground acceleration (g)
		Common parameters	Shear modulus G (kN/m^2)	Shear wave velocity Vs (m/s)	Unit volume weight	Shear modulus G (kN/m^2)	Structure depth d (m)	
Ground surface ～ -1.0m	1.0m	Unit volume weight 1.86 tf/m^3 Cohesion C 3kPa Friction angle ϕ 30° Poisson's ratio ν 0.40 Damping ratio 3%	1.860×10^4	100	0.85 tf/m^3	3.903×10^6	5.0	0.3
-1.0m ～ -3.5m	2.5m		3.143×10^4	130				
-3.5m ～ -7.5m	4.0m		5.375×10^4	170				
-7.5m ～ -13.5m	6.0m		6.175×10^4	190				
-13.5m ～ -17.0m	3.5m		1.071×10^5	240				

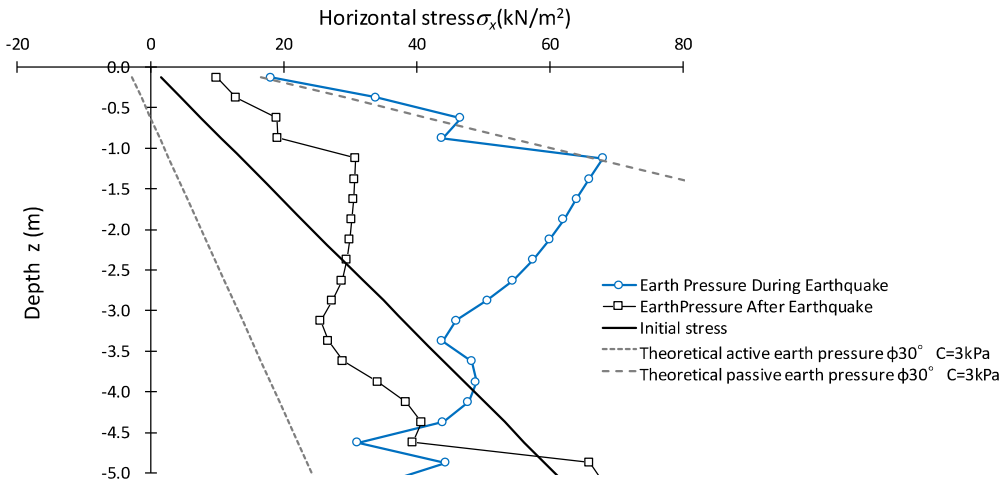

Fig. 12– Depth-wise distributions of σ_x for for comparing with conventional desgin methods

8. Conclusion

In recent times, semi-underground structures, whose most part is placed underground and the roofs are covered with thin or no soil layers, are often constructed. Most of these structures are lighter and stiffer than the surrounding soil. We investigate dynamic interaction mechanism between ground and side wall of semi-underground structures on the basis of two-dimensional FEM analysis. The earth pressure acting on semi-underground structures should be governed by the effects of both inertia and kinematic interaction. In order to make the mechanism clear, non-mass and rigid structures are studied, which give the maximum interaction.

The spatial distributions of horizontal stress normalized by the initial values were studied. The results show that in the area near the structural wall, active and passive states appear alternatively take turns reciprocally during shaking. After shaking, the stress do not return to the initial values, which stays passive in the shallow area and active in the deep area. The depth-wise distribution of σ_x acting on the structural wall and its extended deeper plane, were also studied. Passive earth pressure acts on the shallow part of the wall whereas active earth pressure acts on the deeper part, during earthquake. The residual earth pressure, which is approximately the median value of active and passive earth pressure, acts after earthquake.

Parameter study has been performed considering the surface layer thickness, structural depth, and predominant period and amplitude of input motion. To understand the effect of parameters, the depth is normalized by structural depth and the horizontal stress is converted to Rankine's coefficient of earth pressure. The values of coefficient vary between K_p and K_a, Rankine's coefficient of passive and active earth pressure, respectively. Depth-wise distribution of the coefficient is not affected by the surface soil thickness. The amplitude of input motion determines the area in which the passive earth pressure acts, whereas its period has little effect on the distribution.

It is found that the conventional design methods could not represent the complex distribution of earth pressure acting on the semi-underground structure obtained by non-linear FEM. The maximum and residual distributions of earth pressure during earthquakes are also examined using the practical conditions. The conclusions obtained from the simple conditions are confirmed.

It is necessary to develop a standard design method considering the detailed mechanism of earth pressure in order to design the semi-underground structures properly.

6. References

[1] Sano, T. (1916) : Theory of earthquake resistant structures of houses. *Association for Earthquake Disaster Prevention*, Vol.83, 1-15.

[2] Okabe, S. (1924) : General theory of earth pressure and seismic stability of retaining wall and dam. *J.JSCE, Vol.10 No.6*.

[3] Mononobe, N., and Matsuo, H. (1929) : On the determination of earth pressures during earthquakes. *Proceeding of the World Engineering Congress*, Tokyo, Japan, Vol.9, paper no. 388, 177-185.

[4] Wood, J. H. (1973) : Earthquake-induced soil pressures on structures. *Earthquake Engineering Research Laboratory*, California Inst. of Technol., Pasadena, Calif., Rep. EERL 73-05.

[5] Koseki, J., Tatsuoka, F., Munaf, Y., Tateyama, M., Kojima, K. (1998) : A modified procedure to evaluate earth pressure at high seismic load. *Spatial Issue of Soils and Foundation*, 209-216.

[6] Tokyo Metropolitan Waterworks (2013): *Seismic design Guidelines*, PP. 16.

[7] Towhata, I. (2008): *Geotechnical Earthquake Engineering*, PP. 248.

[8] Murai, K., Otsuka, H., Yabuki, W. (2000) : Study on the accuracy of seismic deformation method focusing on external forces and the interaction spring. *Proceedings of tunnel engineering*, *JSCE., Vol.10*, PP. 79-86.

[9] Katayama, I. (1990) : Studies on Fundamental Problems in Seismic Design Analyses of Critical Structures and Facilities. *Ph. D. Dissertation*, Kyoto University, 188-237.

[10] Towhata, I. (2008): *Geotechnical Earthquake Engineering*, PP. 255.

[11] Siba, Y. (2013) : A theoretical study on the analytical model used in the seismic design for underground vertical shaft structures. *J.JSCE A1 Vol.69, No4*, I_55-I_72.

[12] Sitar, N., Geraili, R., Candia, G. (2012) : Seismically Induced Lateral Earth Pressures on Retaining Structures and Basement Walls. *Keynote Lecture, Geotechnical Engineering State of the Art and Practice, Keynote Lectures from Geo Congr*.

[13] Lohrasb, K., Anne, L. (2019) : Experimental studies of seismic soil pressures on vertical flexible, underground structures and analytical comparisons. *Soil Dynamics and Earthquake Engineering 118*, 166–178.ess, GSP 226, ASCE.

[14] Veletsos, A. S., Younan. A. H. (1994) : Dynamic soil pressure on rigid vertical walls. *Earthquake Engineering and Structural Dynamics, 23*, 275–301.

[15] Veletsos, A. S., Younan. A. H. (1997) : Dynamic response of cantilever retaining walls. *Journal of Geotechnical and Geoenvironmental Engineerings, Vol. 123*, Issue 2.

[16] Inoko, K., Ohtake, K., Narita, K., Ariga, K., Hayakawa, M. (2013) : Influence of surface subsoil hardness on earthquake behavior of RC tanks. *J.JSCE A1 Vol.71, No4*, I_832-I_845.

[17] Tokyo Metropolitan Waterworks (2013) : *Seismic design Guidelines*, PP. 8.

[18] Igarashi, T., Sawada, S., Goto, H. : Earth Pressure Acting on Semi underground structures and After Earthquakes. *J.JSCE*, (submitted).

[19] Seed, H, B., Idriss, I, M. (1970) : Soil moduli and damping Factors for dynamic response analysis. *Earthquake Engineering Research Center,* Report No. EERC70-10.

[20] Nakamura, Y. (2000), : Evaluation of Damage Mechanism of Subway Station Based on The Difference Damage Between Two Damaged Subway Stations Due to The Earthquake. *J.JSCE No654,* I-52,335-354.

[21] Japan Water Works Association (2009), *Guidelines of Earthquake Proof Construction Method for Waterworks Facilities*, PP. 250.

